Electric dipole and quadrupole transition amplitudes for Ba^+ using the relativistic coupled-cluster method

Geetha Gopakumar, Holger Merlitz, Rajat K. Chaudhuri, and B. P. Das
Non-Accelerator Particle Physics Group, Indian Institute of Astrophysics, Bangalore 560034, India

Uttam Sinha Mahapatra and Debashis Mukherjee
Indian Association for Cultivation of Science, Calcutta 700032, India

(Received 13 November 2001; revised manscript received 7 June 2002; published 27 September 2002)

We present our calculations of the electric dipole and quadrupole matrix elements for transitions between low-lying bound states of Ba^+ that are relevant for parity nonconservation studies using the relativistic coupled-cluster method. The results compare well with the experimental data. We have also computed the electric dipole transition matrix elements between many high-lying excited states.

DOI: 10.1103/PhysRevA.66.032505 PACS number(s): 31.15.Dv, 32.10.Dk, 31.25.Jf

I. INTRODUCTION

High precision calculations to the level of less than 1% are currently of interest in a number of different contexts in atomic physics. One among them is the continuous attempts at improving the accuracy of powerful many-body theories, such as the coupled-cluster method (CCM) [1–3], that are applied to atomic systems for calculating various properties. Also the combined precision between theory and experiment to this level is necessary to arrive at conclusions regarding the underlying physics for a variety of problems. Parity nonconservation in atoms and ions is an important area of atomic physics where accurate theoretical calculations [4–6] combined with experiments [7,8] can give important information about the possible existence of new physics beyond the standard model in the regime of small momentum transfer [9]. To date, such precision has been achieved only for atomic Cs [6]. The parity nonconservation (PNC) induced transition matrix element connecting states of mixed parity depends on the region near as well as far away from the nucleus due to the properties of the PNC and the electric dipole operators.

An experiment to observe parity nonconservation using the $|5p^6 6s\rangle_{1/2} \rightarrow |5p^6 5d\rangle_{3/2}$ transition in Ba^+ has been proposed by Fortson [10]. There have been theoretical calculations on this ion using the configuration-interaction (CI) method [11,12] and many-body perturbation theory (MBPT) [13]. In order to determine the accuracy of the PNC calculations, it is necessary to know the accuracy to which one can calculate the electric dipole, and the PNC matrix elements as well as the excitation energies. We had presented our excitation energy calculations for the low-lying levels of Ba^+ using the relativistic CCM in a recent paper [14]. These results have been computed to an accuracy of less than 0.2% for ionization potentials and 0.6% for excitiaton energies. In this paper we attempt to determine the accuracy of wave functions at large radial distances by computing the electric dipole transition amplitudes that are relevant for PNC in Ba^+. As the PNC observable for this ion arises from the interference between parity nonconserving electric dipole and allowed electric quadrupole amplitudes for the aforementioned transition, we have also calculated the latter.

In Sec. II, we describe our CCM-based approach to the calculation of the all order matrix elements and in Sec. III we present the numerical results obtained for the matrix elements.

II. METHOD OF CALCULATION

Since we are dealing with Ba^+ $(Z=56)$ in this work, we consider the Dirac-Coulomb (DC) Hamiltonian given by

$$H_{DC}=\sum_i^N \left[c\,\alpha_i \cdot p_i + (\beta_i - 1)c^2 + V_{nuc}(r_i) + \sum_{i<j} \frac{1}{r_{ij}} \right]. \tag{1}$$

Breit interaction and radiative corrections are not considered in the present work as their contributions are rather small compared to the terms present in the DC Hamiltonian.

In our calculations we start with the Dirac-Fock (DF) reference state corresponding to the $N-1$ electron closed-shell configuration. To this we add one electron to the kth virtual orbital and obtain the N electron system on which calculations are carried out. The addition of a valence electron to the kth virtual orbital of the reference state can therefore be written as

$$|\Phi_k^N\rangle = a_k^\dagger |\Phi_0\rangle, \tag{2}$$

where $|\Phi_0\rangle$ is the DF reference state. Any general state can be written in open-shell CCM [1] as

$$|\Psi_k^N\rangle = \{e^{S_k^{(0)}}\} e^{T^{(0)}} |\Phi_k^N\rangle, \tag{3}$$

where T is the operator describing excitations from the core and S the excitations from core and the valence to virtual orbitals. Using the mathematical simplifications given in [14], we arrive at two different equations for determining the

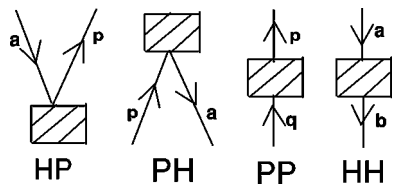

FIG. 1. Form of effective $\bar{O}$ one-body diagrams.

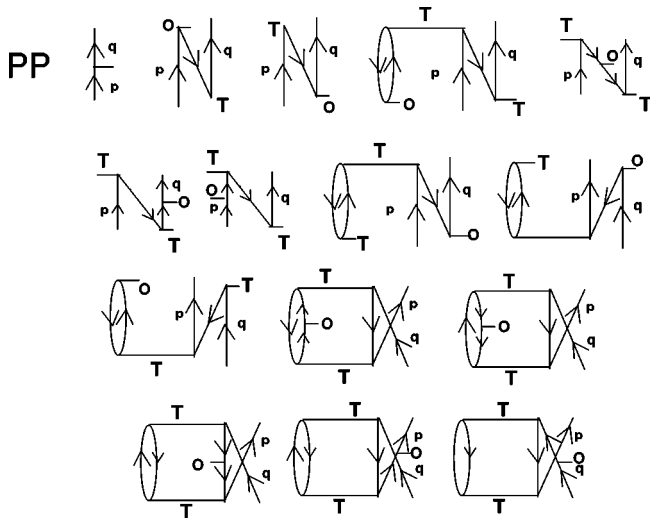

FIG. 2. Typical effective one-body diagrams ($\overline{O}$) for a one-body operator. Exchange diagrams are not shown.

T and the S amplitudes using the CC formalism. In the present work we have used the coupled-cluster singles, doubles, and partial triples [CCSD(T)] formalism for determining the T and S amplitudes [14]. Once the T and S amplitudes are known, we can compute the matrix elements as discussed by [15]. If we consider O to be a general single-particle operator, then the matrix element of the operator O between an initial and final state is given by

$$O_{fi}=\frac{\langle\Psi_f|O|\Psi_i\rangle}{\sqrt{\langle\Psi_f|\Psi_f\rangle}\sqrt{\langle\Psi_i|\Psi_i\rangle}}. \tag{4}$$

Substituting the CC wave functions, we get

$$O_{fi}=\frac{\langle\Phi_f|e^{\{S_f^+\}}e^{T^\dagger}Oe^{T}e^{\{S_i\}}|\Phi_i\rangle}{\sqrt{\langle\Phi_f|e^{\{S_f^\dagger\}}e^{T^\dagger}e^{T}e^{\{S_f\}}|\Phi_f\rangle}\sqrt{\langle\Phi_i|e^{\{S_i^\dagger\}}e^{T^\dagger}e^{T}e^{\{S_i\}}|\Phi_i\rangle}}. \tag{5}$$

We first evaluate the quantity $e^{T^\dagger}Oe^{T}=\overline{O}$ which can be expanded using the Hausdorff relation [16]. Here we consider the effective one-body $\overline{O}$ diagrams of the kind given in Fig. 1, where P refers to virtual and H refers to core orbitals.

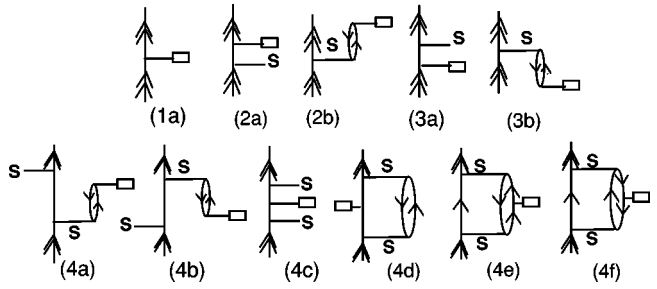

FIG. 3. Diagrams contributing to the numerator of Eq. (5) where the effective one-body $\overline{O}$ (here a box denotes $\overline{O}$) is sandwiched between the S operators. Exchange diagrams are not shown. (1a) $\langle f|\overline{O}|i\rangle$; (2a,2b) $\langle f|\overline{O}S_i|i\rangle$; (3a,3b) $\langle f|S_f^\dagger\overline{O}|i\rangle$; (4$a$,4$b$,4$c$,4$d$,4$e$,4$f$) $\langle f|S_f^\dagger\overline{O}S_i|i\rangle$.

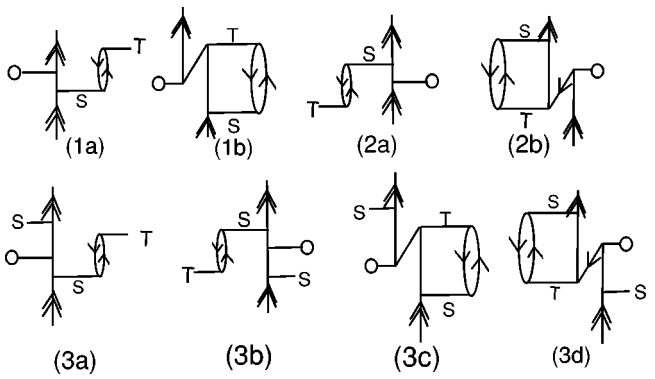

FIG. 4. Diagrams contributing to the numerator of Eq. (5) where effective two-body $\overline{O}$ (here the circles denote O) is sandwiched between the S operators. Exchange diagrams are not shown. (1a)(1b) $\langle f|\overline{O}S_i|i\rangle$; (2a,2b) $\langle f|S_f^\dagger\overline{O}|i\rangle$; (3a,3b,3c,3d) $\langle f|S_f^\dagger\overline{O}S_i|i\rangle$.

Typical one-body PP diagrams generated from the two terms $OT_1, T_2^\dagger OT_1$ and their adjoints and also $T_1^\dagger OT_1$ and $T_2^\dagger OT_2$ are given in Fig. 2. Similar diagrams can be drawn corresponding to HH, PH, and HP.

We have also considered the dominant part of the effective two-body $\overline{O}$ diagrams which are constructed from the terms $T_1^\dagger O$ and $T_2^\dagger O$ and their adjoints. The rest of the diagrams have not been included in the present calculation. These effective one- and two-body diagrams are then sandwiched between the S operators. The numerator in Eq. (5) therefore has terms of the form $\langle f|\overline{O}|i\rangle$, $\langle f|[S^\dagger\overline{O}]_c|i\rangle$, $\langle f|[\overline{O}S]_c|i\rangle$, and $\langle f|[S^\dagger\overline{O}S]_c|i\rangle$, where c refers to completely connected diagrams. Here we consider a maximum of four amplitudes in the numerator of the Eq. (5) inclusive of the T and S amplitude for the one-body $\overline{O}$ and three amplitudes for the two-body $\overline{O}$ diagrams. Contraction of the effective one-body and two-body terms with the S and $S^\dagger$ amplitudes leads to 18 diagrams each. Typical diagrams from effective one- and two-body $\overline{O}$ are given in Figs. 3 and 4.

The square of the denominator in Eq. (5) takes the form

$$N^2=\langle\Phi_0|a_k\{1+S_k^\dagger\}^\dagger(1+T^\dagger+[T^\dagger T]_c+\cdots)\times\{1+S_k\}a_k^\dagger|\Phi_o\rangle, \tag{6}$$

where "c" denotes completely connected diagrams. The effect of this denominator is to cancel disconnected terms from the numerator. This cancellation is complete for closed-shells and it has been shown by Blundell *et al.* [17] that for the single valence states there is a residual normalization correction given by

TABLE I. Number of Gaussian basis functions used for the computation of orbitals of each symmetry for Ba^+.

$s(1/2)$	$p(1/2,3/2)$	$d(3/2,5/2)$	$f(5/2,7/2)$	$g(7/2,9/2)$	$h(9/2,11/2)$
32	28	25	20	15	10

TABLE II. Orbital generation.

Symmetry -	No. of orbitals in each symmetry	Numerical orbitals used in the calculation	Gaussian orbitals used in the calculation
$s(1/2)$	9	$3s,4s,\ldots,8s$	$9s,\ldots,11s$
$p(1/2,3/2)$	9	$3p,\ldots,8p$	$9p,\ldots,11p$
$d(3/2,5/2)$	10	$3d,\ldots,7d$	$8d,\ldots,12d$
$f(5/2,7/2)$	9	$4f,5f$	$6f,\ldots,12f$
$g(7/2,9/2)$	9	-	$5g,\ldots,13g$
$h(9/2,11/2)$	7	-	$6h,\ldots,12h$

$$\langle\Phi_f|e^{\{S_f^+\}}e^{T^\dagger}Oe^{T}e^{\{S_i\}}|\Phi_i\rangle\left[\frac{1}{\sqrt{\langle\Psi_f|\Psi_f\rangle}\sqrt{\langle\Psi_i|\Psi_i\rangle}}-1\right]. \quad (7)$$

The possible diagrams given in Fig. 3 can be classified as DF, random phase approximation (RPA), Bruckner correlation, structural radiation, and the correction due to normalization. A very elaborate description of the above types of corrections with the associated diagrams are given in the paper by Blundell *et al.* [15]. The T part of Eq. (6) gives rise

TABLE III. Reduced electric dipole and quadrupole matrix elements in length form for the Ba^+ ion. Here $\overline{O}_1$ and $\overline{O}_2$ denotes one- and two-body $\overline{O}$ diagrams. MBPT(1) is first-order MBPT, D is dipole, and Q is quadrupole.

Transition	DF	DF+MBPT(1)	$\overline{O}_1$	$[S^+\overline{O}_1]_c$	$[\overline{O}_1S]_c$	$(S^+\overline{O}_1S)_c$	$(S^+\overline{O}_2)_c$	$(\overline{O}_2S)_c$	$(S^+\overline{O}_2S)_c$	Norm.	D matrix
$6s_{1/2}-6p_{1/2}$	3.8909	3.4729	3.8922	−0.3586	−0.1667	0.0543	−0.0009	−0.0018	−0.00004	−0.05714	3.3266
$6s_{1/2}-7p_{1/2}$	0.0654	−0.1151	0.0657	0.4120	−0.3554	0.0157	−0.0003	−0.0018	0.0002	−0.0019	0.1193
$6s_{1/2}-8p_{1/2}$	−0.0071	−0.1214	−0.0053	−0.2825	−0.1713	−0.0103	−0.0002	0.0023	0.0002	0.0057	−0.4696
$7s_{1/2}-6p_{1/2}$	−2.5487	−2.6082	−2.5481	−0.3152	0.5197	−0.0011	0.0002	−0.0002	0.0000	0.0289	−2.3220
$7s_{1/2}-7p_{1/2}$	7.3917	7.2412	7.3918	−0.1130	0.1350	0.0100	−0.0008	−0.0017	0.0001	−0.0825	7.3300
$7s_{1/2}-8p_{1/2}$	0.1989	0.1132	0.1998	−0.3792	−0.4501	0.0263	−0.0002	0.0013	0.0002	0.0045	−0.6021
$8s_{1/2}-6p_{1/2}$	0.3806	0.4015	0.3793	0.0113	0.3228	0.0149	−0.0011	0.0002	−0.00001	−0.0065	0.7283
$8s_{1/2}-7p_{1/2}$	1.2751	1.2993	1.2744	0.2653	0.5570	−0.0017	−0.0008	0.0004	−0.0001	−0.0160	2.0804
$8s_{1/2}-8p_{1/2}$	8.3436	8.3686	8.3428	0.0679	−0.1238	−0.0218	−0.0009	−0.0011	−0.00003	−0.0329	8.2315
$6s_{1/2}-6p_{3/2}$	−5.4776	−4.9108	−5.4795	0.5248	0.2046	−0.0738	0.0005	0.0027	−0.00004	0.0764	−4.6982
$6s_{1/2}-7p_{3/2}$	−0.2610	−0.0072	−0.2613	−0.5742	0.4690	−0.0231	0.0001	0.0028	−0.0004	0.0055	−0.3610
$6s_{1/2}-8p_{3/2}$	−0.0786	0.0838	−0.0810	0.3973	0.2409	0.0121	0.0001	−0.0031	−0.0003	−0.0068	0.5710
$7s_{1/2}-6p_{3/2}$	3.9567	4.0217	3.9558	0.4381	−0.7154	0.0049	−0.0007	0.0003	0.0001	−0.0420	3.6482
$7s_{1/2}-7p_{3/2}$	−10.3120	−10.1116	−10.3121	0.1658	−0.2319	−0.0094	0.0010	0.0025	−0.0002	0.1081	−10.2645
$7s_{1/2}-8p_{3/2}$	−0.5675	−0.4504	−0.5687	0.5702	0.5848	−0.0354	0.0002	−0.0018	−0.0002	−0.0040	0.5514
$8s_{1/2}-6p_{3/2}$	−0.5521	−0.5739	−0.5499	−0.0011	−0.4875	−0.0211	0.0017	−0.0003	−0.00002	0.0084	−1.0518
$8s_{1/2}-7p_{3/2}$	−1.8334	−1.8610	−1.8322	−0.3699	−0.8347	0.0045	0.0013	−0.0007	0.0001	0.0211	−3.0172
$8s_{1/2}-8p_{3/2}$	−12.7376	−12.7672	−12.7363	−0.1041	0.1615	0.0283	0.0014	0.0016	0.00005	0.0458	−12.6033
$5d_{3/2}-6p_{1/2}$	−3.7454	−3.3883	−3.7475	0.6913	0.0772	−0.0602	−0.0015	0.0010	−0.0003	0.0645	−2.9449
$5d_{3/2}-7p_{1/2}$	−0.3513	−0.1946	−0.3525	−0.1850	0.2799	−0.0185	−0.0005	0.0004	−0.0001	0.0062	−0.3050
$5d_{3/2}-8p_{1/2}$	−0.19563	−0.0953	−0.1966	−0.0636	0.1560	−0.0190	−0.0002	0.0002	−0.0001	0.0019	−0.1121
$5d_{3/2}-6p_{3/2}$	−1.6354	−1.4917	−1.6358	0.3137	0.0257	−0.0254	−0.0012	0.0004	−0.0001	0.0269	−1.2836
$5d_{3/2}-7p_{3/2}$	−0.1864	−0.1226	−0.1866	−0.0701	0.1130	−0.0297	−0.0005	0.0002	−0.00004	0.0032	−0.1645
$5d_{3/2}-8p_{3/2}$	−0.1019	−0.0611	−0.1022	−0.0240	0.0658	−0.0094	−0.0002	0.0001	−0.00003	0.0011	−0.0650
$5d_{5/2}-6p_{3/2}$	−5.0011	−4.5697	−5.0021	0.9152	0.0772	−0.0770	−0.0034	0.0012	−0.0005	0.0660	−3.9876
$5d_{5/2}-7p_{3/2}$	−0.5425	−0.3530	−0.5429	−0.2149	0.3431	−0.0878	−0.0014	0.0005	−0.0002	0.0073	−0.4788
$5d_{5/2}-8p_{3/2}$	−0.2976	−0.1762	−0.2981	−0.0777	0.1977	−0.0273	−0.0007	0.0002	−0.0001	0.0024	−0.1926

Transition	DF	DF+MBPT(1)	$\overline{O}_1$	$[S^+\overline{O}_1]_c$	$[\overline{O}_1S]_c$	$[S^+\overline{O}_1S]_c$	$[S^+\overline{O}_2]_c$	$[\overline{O}_2S]_c$	$[S^+\overline{O}_2S]_c$	Norm.	Q matrix
$6s_{1/2}-5d_{3/2}$	14.7633	14.5582	14.7619	−0.3387	−1.9384	0.1532	−0.0051	0.0035	0.0006	−0.0799	12.6251
$6s_{1/2}-5d_{5/2}$	−18.3840	−18.1581	−18.3794	0.4151	2.3787	−0.2221	0.0064	−0.0041	−0.0007	0.0703	−15.7832
$7s_{1/2}-5d_{3/2}$	−6.1995	−6.2751	−6.1994	−0.9615	3.0868	0.1735	−0.0012	0.0021	0.0003	0.0270	−3.9021
$7s_{1/2}-5d_{5/2}$	7.9363	8.0165	7.9373	1.1903	−3.7278	−0.1998	0.0014	−0.0025	−0.0004	−0.0262	5.2072

TABLE IV. Electric dipole matrix elements in different transitions for Ba^+ and the comparison of transition probabilities with experimental values.

Transition	Present work		[21]	[21]	[13]	Expt.	Expt.
	D (a.u.)	$A_{fi}\times10^9$ sec^{-1}	D (a.u.)	$A_{fi}\times10^9$ sec^{-1}	$A_{fi}\times10^9$ sec^{-1}	$A_{fi}\times10^9$ sec^{-1}	D(a.u)
$6s_{1/2}-6p_{1/2}$	3.3266	0.09368	3.300	0.09178	0.092327	0.095±0.009,[a] 0.0955±0.0010,[b] 0.095±0.007[c]	3.3664[b]
$6s_{1/2}-6p_{3/2}$	4.6982	0.11937	4.658	0.11625	0.117066	0.106±0.009,[a] 0.117±0.004,[b] 0.118±0.008[c]	4.6729[b]
$5d_{3/2}-6p_{3/2}$	1.2836	0.004255	1.312	0.00435	0.004492	0.00469±0.00029,[a] 0.0048±0.0005,[b] 0.0048±0.0006[c]	1.3633[a]
$5d_{5/2}-6p_{3/2}$	3.9876	0.03493	4.057	0.03595	0.034453	0.0377±0.0024,[a] 0.037±0.004,[b] 0.037±0.004[c]	4.1547[a]
$5d_{3/2}-6p_{1/2}$	2.9449	0.032609	3.009	0.03342	0.037033	0.0338±0.00019[a] 0.0333±0.008[b] 0.033±0.004[c]	3.0262[a]

[a]Reference [22].
[b]Reference [23].
[c]Reference [24].

to possible diagrams of the type PP, HP, PH, and HP as shown in Fig. 1. After connecting these diagrams to the S operator, one obtains the kind of diagrams shown in Fig. 3 with the open lines denoted by v and v' being identical and with the $\overline{O}$ interchanged with the connected effective one-body T part. The expression for the single-particle electric dipole and quadrupole transition matrix elements and transition probability are given in Appendices A and B.

III. RESULTS AND DISCUSSION

In the present calculation, the single-particle DF orbitals are generated with Ba^{++} $(5p^6)$ as the starting potential. We make use of a hybrid approach [18] where we consider a part numerical and part analytical orbitals on a grid. The analytical orbitals (in this case Gaussian-type orbitals) are generated using the finite basis-set expansion (FBSE) method [19] and the numerical orbitals from the general purpose relativistic atomic structure program (GRASP) [20]. The number of analytical orbitals used for the generation of orbitals of different symmetry is given in Table I.

For the coupled-cluster calculations, we have restricted the basis by imposing upper and lower bounds in energy for the single-particle orbitals as -100 a.u. and 100 a.u. for all symmetries except h. The reason for choosing such a basis is explained in our previous paper [14]. The number of analytical and numerical orbitals used for this calculation is tabulated in Table II.

In this calculation the effective one- and two-body $\overline{O}$ terms are first computed and later on sandwiched between the S operators. This leads to terms of the form $\langle f|\overline{O}|i\rangle$,$\langle f|S_f^\dagger\overline{O}|i\rangle$,$\langle f|\overline{O}S_i|i\rangle$, and $\langle f|S_f^\dagger\overline{O}S_i|i\rangle$. In Table III the contribution from different terms classified as above for the effective one- and two-body $\overline{O}$ are given separately. The correlation corrections to the DF term $\langle f|O|i\rangle$ contributing to $\langle f|\overline{O}|i\rangle$ represented in Fig. 3 as (1a) is found to be less than 0.04% to the total value which has contributions from the DF as well as the correlation effects. The corrections obtained by adding the 5th, 6th, 8th, and 9th columns of Table III, represented in Fig. 3 as (2a,2b,3a,3b) and in Fig. 4 as (1a,1b,2a,2b), contributes $\sim$20% and the sum of the terms tabulated in the 7th and 10th columns of Table III, represented in Fig. 3 as (4a,4b,4c,4d,4e,4f) and in Fig. 4 as (3a,3b,3c,3d), contributes $\sim$2%. The normalization correction given in the 11th column contributes $\sim$2%. The effective one- and two-body $\overline{O}$ diagrams contributing to the above terms is around 14% and 0.1%. This indicates that the omission of the other two-body diagrams contribute less than

TABLE V. Lifetimes of states of Ba^+ computed using theoretical $E1/E2$ transition amplitudes.

State	Present work (nsec)	Guet [21] (nsec)	Dzuba [13] (nsec)	Expt. (nsec)
$6p(1/2)$	7.92	7.99	7.89	7.90(10) [a]
$6p(3/2)$	6.31	6.39	6.30	6.32(10) [a]
State	**Present work (sec)**	**Guet [21] (sec)**	**Dzuba [13] (sec)**	**Expt. (sec)**
$5d(3/2)$	81.4	83.7	81.5	79.8(4.6) [b]
$5d(5/2)$	36.5	37.2	30.3	34.5(3.5) [c]

[a]Reference [27].
[b]Reference [28].
[c]Reference [29].

TABLE VI. Theoretical and experimental energy differences between the ground and the excited state of Ba^{++}.

State	Present work (cm^{-1})	Guet [21] (cm^{-1})	Dzuba [13] (cm^{-1})	Kaldor [30] (cm^{-1})	Experiment (cm^{-1})
$6s-6p(1/2)$	20293	20995	20232	20396	20262
$6s-6p(3/2)$	22020	22742	21953	22103	21952
$6s-5d(3/2)$	4809	4688	4411	5268	4874
$6s-5d(5/2)$	5713	5620	5288	6093	5675

0.1% to the electric dipole and quadrupole matrix elements. We have considered various transitions involving low-lying levels and high-lying levels like $7s(1/2)$,$8s(1/2)$, $7p(1/2,3/2)$, and $8p(1/2,3/2)$ states.

Using the all order $E1$ matrix elements, the transition probabilities were calculated using the expressions given in Appendix B. The above transition probabilities are compared with experimental data and calculations by Guet *et al.* [21] and Dzuba *et al.* [13] in Table IV. These two calculations have certain semiempirical features in the evaluation of pair correlation effects, while as mentioned in Sec. II, we have used a completely *ab initio* approach based on the nonlinear CCSD(T) method. Here the calculations were restricted to the low-lying levels, $6s(1/2)$, $6p(1/2,3/2)$, and $5d(3/2,5/2)$.

The electric dipole transition amplitude induced by PNC (E1PNC) from $|5p^6 6s_{1/2}\rangle \rightarrow |5p^6 5d_{3/2}\rangle$ for Ba^+ using the sum over states approach [25] can be written as

$$\mathrm{E1PNC} = \frac{1}{\left(\sqrt{\langle\Psi_i^{(0)}|\Psi_i^{(0)}\rangle}\sqrt{\langle\Psi_f^{(0)}|\Psi_f^{(0)}\rangle}\right)} \times \sum_I \left(\frac{\langle\Psi_f^{(0)}|D|\Psi_I^{(0)}\rangle\langle\Psi_I^{(0)}|\mathrm{PNC}|\Psi_i^{(0)}\rangle}{(E_i - E_I)} + \frac{\langle\Psi_f^{(0)}|H_{\mathrm{PNC}}|\Psi_I^{(0)}\rangle\langle\Psi_I^{(0)}|D|\Psi_i^{(0)}\rangle}{(E_f - E_I)} \right). \quad (8)$$

From angular momentum considerations, we know that the nuclear spin independent (NSI) [11,12] PNC (rank zero tensor) can connect only states of the same angular momentum. Hence, the first term in the E1PNC expression can have intermediate atomic state functions with angular momentum $j = 1/2$ and the second term with angular momentum $j = 3/2$. For Ba^+ [13,26] it is clear that the largest contribution to E1PNC for $|5p^6 6s\rangle_{1/2} \rightarrow |5p^6 5d\rangle_{3/2}$ results from $|5p^6 6p\rangle_{1/2}$ and $|5p^6 6p\rangle_{3/2}$ intermediate states, respectively, for the first and second terms. Hence, accuracy of the E1PNC calculation mainly depends on the matrix elements $\langle 5p^6 5d_{3/2}|D|5p^6 6p_{1/2}\rangle$, $\langle 5p^6 6p3/2|D|5p^6 6s_{1/2}\rangle$, $\langle 5p^6 6p_{1/2}|\mathrm{PNC}|5p^6 6s_{1/2}\rangle$, $\langle 5p^6 5d3/2|\mathrm{PNC}|5p^6 6p_{3/2}\rangle$, and the energy differences $E_{5p^6 6s_{1/2}} - E_{5p^6 6p_{1/2}}$ and $E_{5p^6 5d_{3/2}} - E_{5p^6 6p_{3/2}}$. Also the physical quantity that has been proposed to be measured in the PNC experiment on Ba^+ currently underway at the University of Washington, Seattle is a parity nonconserving light shift (ac Stark shift) arising from the interference of the parity nonconserving electric dipole transition amplitude and the electric quadrupole transition amplitude ($E2$). Therefore in addition to E1PNC, an accurate calculation of the $E2$ matrix element between $|5p^6 6s\rangle_{1/2}$ and $|5p^6 5d\rangle_{3/2}$ states is also necessary.

From the experimental transition probablities and excitation energies, the electric dipole matrix elements for the allowed $E1$ transitions were obtained and compared with our calculated electric dipole matrix elements. The results are given in Table IV. For the electric quadrupole transition connecting $5d_{3/2}$ to $6s_{1/2}$ states, neglecting the $M1$ transition since it is weak [21], the experimental electric quadrupole matrix element was determined from the experimental lifetime and the excitation energy as

$$\langle 5d_{3/2}|E2|6s_{1/2}\rangle = \sqrt{\frac{g_k \lambda^5}{\tau_{5d_{3/2}} 1.1191 \times 10^{18}}}, \quad (9)$$

where λ is the transition wavelength in Å, g_k is the $(2J+1)$ degeneracy of the upper level, and $\tau_{5d_{3/2}}$ is the lifetime of the $5d_{3/2}$ state in the units of sec^{-1}. Using the experimental $\tau_{5d_{3/2}} = 79.8 \pm 4.6$ sec [28], the electric quadrupole matrix element is found to be in the range 12.40 to 13.14 a.u. Our calculated electric quadrupole matrix element for the above-mentioned transition is 12.63 a.u. which is well within the experimental error bar. In Table V we compare the values of the lifetimes obtained from our calculated $E1$ and $E2$ line strengths and experimental excitation energies given in Table VI with the measured lifetimes.

IV. CONCLUSION

We have calculated the electric dipole transition amplitudes for low-lying bound states of Ba^+ and found that they agree well with the experimental values derived from experimental transition probabilities and excitation energies. The calculated electric quadrupole transition amplitude between $5d_{3/2}$ and $6s_{1/2}$ also compares well with the experimental value derived from the lifetime and excitation energy. We find that the dominant contribution to electron correlation effects comes from the one-body $\overline{O}$ diagrams for all the transition amplitudes that we have calculated.

ACKNOWLEDGMENTS

We thank Angom Dilip Singh, Sonjoy Majumder, K.V.P. Latha, and Bijay Kumar Sahoo for useful discussions. This work was done at IIA using the E450 Sun Ultra SPARC machine. We also acknowledge financial support from

the Department of Atomic Energy (No. 37/15/97-R&D.11 1603).

APPENDIX A: ELECTRIC DIPOLE AND/OR QUADRUPOLE MATRIX ELEMENTS

The single-particle matrix elements in length form is calculated in atomic units as

$$u_{mn}=C^L(m,n)\int dr r^L[P_m(r)P_n(r)+Q_m(r)Q_n(r)], \tag{A1}$$

where

$$C^L(m,n)=(-1)^{j_m+1/2}\sqrt{2j_m+1}\sqrt{2j_n+1}\begin{pmatrix} j_m & L & j_n \\ \frac{1}{2} & 0 & -\frac{1}{2}\end{pmatrix}. \tag{A2}$$

Here $L=1$ for electric dipole and $L=2$ for electric quadrupole transitions.

APPENDIX B: TRANSITION PROBABILITIES

The following [31] are used for the calculation of transition probabilities:

$$A_{E1}=\frac{(2.0261\times 10^{18})S_{E1}}{g_k\lambda^3} \tag{B1}$$

and

$$A_{E2}=\frac{(1.1199\times 10^{18})S_{E2}}{g_k\lambda^5}, \tag{B2}$$

where λ is the transition wavelength in Å, g_k is the $(2J+1)$ degeneracy of the upper level, S_{E1} and S_{E2} are the $E1$ and $E2$ line strengths in atomic units ea_o and ea_o^2. This gives the transition probability in the units of $\sec^{-1}$.

[1] I. Lindgren and J. Morrison, *Atomic Many-Body Theory*, 2nd ed. (Springer-Verlag, Berlin, 1986).

[2] E. Eliav, U. Kaldor, and Y. Ishikawa, Phys. Rev. A **52**, 2765 (1990); E. Eliav, U. Kaldor, and Y. Ishikawa, *ibid.* **49**, 1724 (1994); E. Eliav, U. Kaldor, and Y. Ishikawa, *ibid.* **50**, 1121 (1994).

[3] H. Merlitz, G. Gopakumar, R. Chaudhuri, B. P. Das, U. S. Mahapatra, and D. Mukherjee, Phys. Rev. A **63**, 022507 (2001).

[4] V. A. Dzuba, V. V. Flambaum, and O. P. Sushkov, Phys. Lett. A **141**, 147 (1989); S. A. Blundell, W. R. Johnson, and J. Sapirstein, Phys. Rev. Lett. **65**, 1411 (1990); Phys. Rev. D **45**, 1602 (1992).

[5] A. Derevianko, Phys. Rev. Lett. **85**, 1618 (2000); M. G. Kozlov, S. G. Porsev, and I.I. Tupitsyn, *ibid.* **86**, 3260 (2001); A. Derevianko, Phys. Rev. A **65**, 012106 (2002); A. I. Milstein and O. P. Sushkov, e-print hep-ph/0109257; W. R. Johnson, I. Bednyakov, and G. Soff, Phys. Rev. Lett. **87**, 233001 (2001).

[6] V. A. Dzuba, V. V. Flambaum, and J. S. M. Ginges, e-print hep-ph/0204134.

[7] C. S. Wood, S. C. Bennett, D. Cho, B. P. Masterson, J. L. Robers, C. E. Tanner, and C. E. Wieman, Science **275**, 1759 (1997).

[8] S. C. Bennett and C. E. Wieman, Phys. Rev. Lett. **82**, 2484 (1999).

[9] V. V. Flambaum, in *Symmetries in Subatomic Physics*, edited by X.-H. Guo, A. W. Thomas, and A. G. Williams, AIP Conf. Proc. No. 539 (AIP, Melville, NY, 2000).

[10] N. Fortson, Phys. Rev. Lett. **70**, 2383 (1993).

[11] Swati Malhotra, Angom D. Singh, and B. P. Das, Phys. Rev. A **51**, R2665 (1995).

[12] K. P. Geetha, Angom D. Singh, and B. P. Das, Phys. Rev. A **58**, R16 (1998).

[13] V. A. Dzuba, V. V. Flambaum, and J. S. M. Ginges, Phys. Rev. A **63**, 062101 (2001).

[14] Geetha Gopakumar, Holger Merlitz, Sonjoy Majumder, Rajat Chaudhuri, B. P. Das, U. S. Mahapatra, and D. Mukherjee, Phys. Rev. A **64**, 032502 (2001).

[15] S. A. Blundell, W. R. Johnson, and J. Sapirstein, Phys. Rev. A **43**, 3407 (1991).

[16] J. J. Sakurai, *Modern Quantum Mechanics*, revised ed. (Addison-Wesley, Reading, MA, 1994).

[17] S. A. Blundell, W. R. Johnson, and J. Sapirstein, Phys. Rev. A **40**, 2233 (1989).

[18] Sonjoy Majumbder, Geetha Gopakumar, Holger Merlitz, and B. P. Das, J. Phys. B (to be published).

[19] R. K. Chaudhuri, P. K. Panda, and B. P. Das, Phys. Rev. A **59**, 1187 (1999).

[20] F. A. Parpia, C. F. Fischer, and I. P. Grant (unpublished).

[21] C. Guet and W. R. Johnson, Phys. Rev. A **44**, 1531 (1991).

[22] A. Kastberg *et al.*, J. Opt. Soc. Am. B **10**, 1330 (1993).

[23] J. Reader *et al.*, *Wavelengths and Transition Probabilities for Atoms and Atomic Ions*, Natl. Bur. Stand. Ref. Data Ser., Natl. Bur. Stand. (U.S.) Circ. No. 68 (GPO, Washington, D.C.), Vol. 10.

[24] A. Gallagher, Phys. Rev. **157**, 24 (1967).

[25] S. A. Blundell, *Applied Many-Body Methods in Spectroscopy and Electronic Structure*, edited by D. Mukherjee (Plenum Press, New York, 1992).

[26] K. P. Geetha, Ph.D thesis, Bangalore University, 2001.

[27] E. H. Pinnington, R. W. Berends, and M. Lumsden, J. Phys. B **28**, 2095 (1995).

[28] N. Yu, W. Nagourney, and H. Dehmelt, Phys. Rev. Lett. **78**, 4893 (1997).

[29] A. A. Madej and J. D. Sankey, Phys. Rev. A **41**, 2621 (1990).

[30] E. Eliav, U. Kaldor, and Y. Ishikawa, Phys. Rev. A **53**, 3050 (1998).

[31] L. I. Sobelman, *Introduction to the Theory of Atomic Spectra* (Pergamon, Oxford, 1972).